Journal of Hydrology (2007) **343**, 43–55

available at www.sciencedirect.com

ScienceDirect

journal homepage: www.elsevier.com/locate/jhydrol

Effect of variable fractal dimension on the floc size distribution of suspended cohesive sediment

F. Maggi [a,*], F. Mietta [b], J.C. Winterwerp [b]

[a] *Civil and Environmental Engineering, 760 Davis Hall, University of California, Berkeley, CA 94720-1710, USA*
[b] *Environmental Fluid Mechanics, Faculty of Civil Engineering and Geosciences, Delft University of Technology, Box 5048, 2600 GA, Delft, The Netherlands*

Received 10 January 2007; received in revised form 23 May 2007; accepted 24 May 2007

KEYWORDS
Flocculation;
Cohesive sediment;
Population balance equation;
Variable fractal dimension

Summary Flocculation of suspended cohesive sediment, well-known to impact the floc size distribution and vertical fluxes, and cause morphodynamic changes of marine and riverine environments, is modelled by means of a population balance equation that implements a novel description of floc geometry: the capacity dimension of fractal flocs, normally assumed constant over the population, has recently been argued to change during flocculation. Our experiments have shown that a power-law function of the dimensionless floc size can conveniently be used to describe these changes. This description of floc capacity dimension is used to explore in detail the extent to which the geometrical properties of flocs affect aggregation and breakup processes, and contribute to shaping their size distribution. A comparison of experimental floc size distributions from settling column test with computed distributions for two hypotheses of floc capacity dimension (i.e., constant and variable) and two hypotheses of flocculation reactions (i.e., semi-stochastic and deterministic) are shown. This suggests that the use of variable rather than constant floc capacity dimension, and the use of semi-stochastic and asymmetric reactions rather than deterministic and symmetric, result in better predictions of the floc size distribution in the environmental conditions herein analysed.

Introduction

Flocculation of cohesive sediment suspended in natural waters is responsible for the small-scale processes of floc genesis and modifications of the floc size distribution. Flocculation also contributes to the meso- and large-scale morphological changes of estuarine environments, coastal zones, canals, rivers and water basins through sediment transport and deposition, which are related to the vertical fluxes of sediment, hence to the floc size and settling velocity distributions. The distributions of size and settling velocity in natural conditions are regulated by many climatological, hydrogeological, biochemical and physical

* Corresponding author.
E-mail address: fmaggi@berkeley.edu (F. Maggi).

0022-1694/$ - see front matter © 2007 Elsevier B.V. All rights reserved.
doi:10.1016/j.jhydrol.2007.05.035

List of symbols

c [ML^{-3}]	sediment concentration
d_0	capacity dimension
e	error function
k	primary particle number
ℓ	dimensionless floc size
p	probability density function
t [T]	time
A [L^{-3}]	aggregation parameter
B_i [L^{-3}]	breakup frequency
E	breakup parameter
F_y [Pa]	floc strength
G [T^{-1}]	turbulent shear rate
L [L]	floc size
L_p [L]	primary particle size
$\alpha_{i,j}$	collision efficiency
$\gamma_{i,j}$	breakup distribution function
δ	primary particle capacity dimension
ξ	rate of change of capacity dimension
η_k [L]	floc primary particle concentration number
η_T [L]	total primary particle concentration number
μ [$ML^{-1}T^{-1}$]	water dynamic viscosity
ρ_s [ML^{-3}]	sediment density
ρ_w [ML^{-3}]	water density
$\Lambda_{i,j}$ [L^3T^{-1}]	collision frequency

processes which exert their impact on the sediment dynamics at manifold time and length scales. One important aspect to the understanding of the overall sedimentological behavior of the suspended sediment is the small-scale particle–particle interaction occurring during flocculation. This is characterised by an interplay between the kinetics of aggregation and breakup reactions, and the geometric and hydraulic properties of individual flocs, which affects the floc size and settling velocity distributions and determine, consequently, the fraction of the sediment that is deposited or transported.

A numerical study of the interplay between the aggregation and breakup precesses and the geometrical properties of sedimentary flocs forming within a population requires the coupling of flocculation dynamics with a model for the geometrical properties of the flocs.

Flocculation of cohesive sediment can be modelled by means of population balance equations (PBEs) that describe the changes in number and composition of flocs within a population, and the factors that influence those changes. The first fundamental work (von Smoluchowski, 1917) focussed on the time variation of the number concentration c of a monodisperse suspension as a function of Brownian diffusion, but no kinematic processes of particle–particle interaction and floc properties were accounted for. Only after several decades, Smoluchowski's equation was extended to compute the floc number concentration in a continuum description of the floc size or volume comprising particle–particle interaction through aggregation and breakup kinetics, and processes of advection, settling, production and loss.

A major feature of these well-established PBEs is that interacting flocs are described either as Euclidean (Friedlander, 1977; McCave, 1984; O'Melia, 1980; Hunt, 1980; Krishnappan, 1990; Lee et al., 1997; Burban et al., 1989; Farley and Morel, 1986) or as fractal bodies with a constant capacity (fractal) dimension regardless of their size or growth state (Flesch et al., 1999; Serra and Casamitjana, 1998b; Zhang and Li, 2003; Kunster et al., 1997). Arguably, as suspended clay minerals are massive crystals while flocs are fluffy, porous and irregularly-shaped bodies, we expect floc geometry to undergo a transition from Euclidean to fractal during growth. While changes in perimeter-based fractal dimension and two-dimensional (2D) capacity dimension are known to appear due to, for example, changes in shear stresses, electrolyte concentration and processes of restructuring, recent works have shown evidences of changes in floc capacity dimension also at stationary environmental conditions and sediment properties, when flocs grow in time (Chakraborti et al., 2003; Maggi, 2007). These findings have raised the need to better implement the fractal description of flocs within a PBE because of a direct role of the floc fractal dimension in particle interactions during aggregation and breakup (e.g., Berka and Rice, 2005; Sato et al., 2004; Li and Logan, 2001; Winterwerp, 1998; Kunster et al., 1997; Veerapaneni and Wiesner, 1996; Burd and Jackson, 1997).

The aim of this paper is to propose the coupling of a Lagrangian population balance equation describing the time evolution of the floc size distribution with a modified model describing statistically self-similar floc geometry. Our working hypotheses are that the floc size does not scale with its mass with an invariant scaling law, i.e., a constant capacity dimension d_0, but that a variant scaling law holds during floc growth, and that the small-scale interplay between the processes of particle aggregation and breakup and geometrical properties of flocs determines the large-scale flocculation dynamics, and the resulting steady state floc size distribution. By means of the mentioned coupling, we will explore the effect of changes in 3D capacity dimension d_0 on the aggregation and breakup kinetics during flocculation, and its impact on the overall floc size distribution.

Our experimental observations suggest that the 3D floc capacity dimension d_0 decreases as a power-law of the dimensionless floc size ℓ. As fractality uniquely relates the size ℓ of a floc to the number of forming primary particles, the structure of the PBE has been elaborated in such a way as to model the suspended matter using the number concentration η_k of flocs formed by k primary particles (i.e., by a mass-based or floc primary-particle number concentration) rather than by the number concentration of flocs with sizes in a given interval. The PBE presented in this work, continuous in time but discrete in η_k, takes into account only processes of aggregation and breakup for reasons of mathematical simplicity, but advection, diffusion, settling, sediment production and loss can straightforwardly be included. The model, calibrated and validated against data obtained from settling column experiments, is analysed for different environmental parameters, and its sensitivity

is explored in detail for different models of floc geometry (constant and variable fractal dimension) and type of reactions (deterministic and stochastic).

Experimental setup

The settling column depicted in Fig. 1 has been used with kaolinite (China clay) sediment with bulk density $\rho_s \approx 2650\ \mathrm{kg/m^3}$, mineral size in the range 0.1—5 μm, and with stable primary particles of size $L_p \approx 5$—$20\ \mu\mathrm{m}$. A highly-concentrated suspension of kaolinite, continuously mixed in the storage tank, is injected into the buffer tank mounted on top of the settling column, and is diluted to the test concentration c via a controlled system which activates an injection pump when the measured mass concentration in the buffer tank is lower than c. Sediment is stirred in the buffer tank with two counter-rotating vanes that produce a re-circulating flow and distribute the particles uniformly when entering the settling column, which is about 5 m high and 300 mm in diameter. Herein, a homogeneous turbulence field, produced by an oscillating three-dimensional grid, induces flocculation. The grid is 4 m high and consists of grid units with a mesh of 75 mm size made with square cross-sectioned rods. Grid units are separated by a distance of 75 mm. Flocs pass through the turbulence field and reach the measuring section under the column, where optical recordings are collected. These are carried out with a particle image system consisting of a high resolution digital camera that records 8-bit gray-scale digital images of 1008-by-1008 pixels, and a laser diode that illuminates flocs from the side with a light sheet. The size of the observation window is 6-by-6 mm, and returns images with 6.42 μm/pixel resolution.

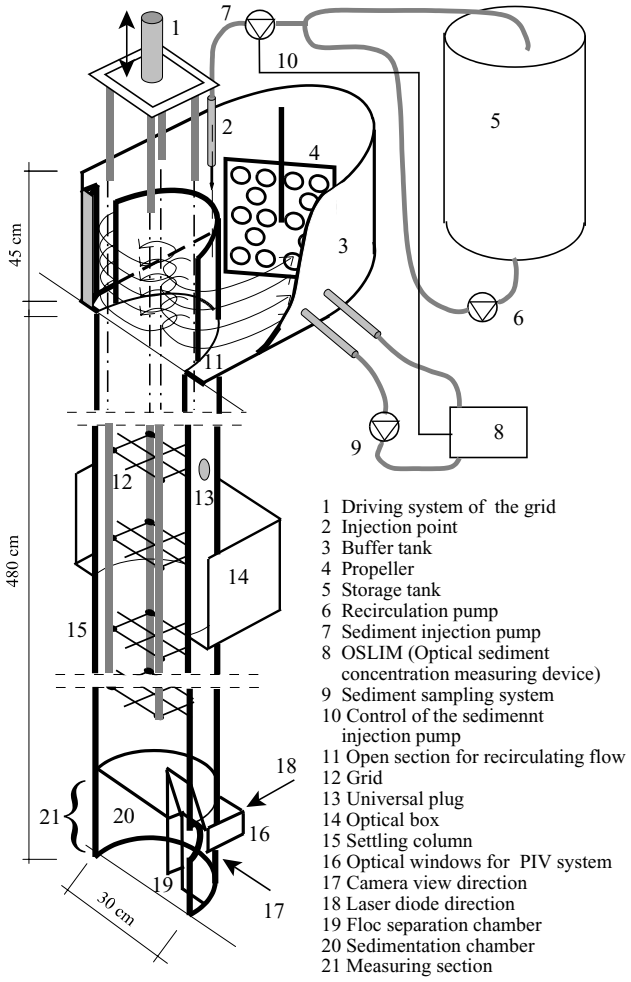

Figure 1 Schematic view of the longitudinal cross-section of the settling column used for laboratory observations (Maggi et al., 2002).

The whole settling column is placed in a climatised room at 18 °C to minimise temperature gradients and convective flows. The experiment is performed with sediment concentration $c = 0.5$ g/l, while the grid is set to oscillate with an amplitude of 84 mm and various frequencies, yielding turbulence shear rates $G = 5, 10, 20, 40\ \mathrm{s^{-1}}$. Three series of images were recorded within a time frame of 3 h for each value of G, which is changed every 12 h to allow the turbulence field and flocculation reactions to reach a steady state. Each series consists of 80 blocks, containing 2 s of recording and 3 s of pause to renew the population in the camera view. Thirty single-frame images were recorded at 15 Hz frequency in each block, and were processed into black-and-white to obtain the FSDs $p(L)$ (Maggi et al., 2006).

Flocculation model

Population balance equation

A Lagrangian population balance equation is used to model cohesive sediment flocs in which the effects of advection, production and loss are neglected assuming that the system is closed (i.e., no mass exchange); the effect of non-linear breakup is neglected too, as this becomes small for low volumetric sediment concentrations (Serra and Casamitjana, 1998b). The variation of the number concentration η_k of flocs made of k primary particles due to aggregation and breakup processes is

$$\frac{d\eta_k}{dt} = \underbrace{\frac{1}{2}\sum_{i=1}^{k-1}\alpha_{i,k-i}\Lambda_{i,k-i}\eta_i\eta_{k-i}}_{\mathscr{G}_{\mathscr{A}}} - \underbrace{\eta_k\sum_{i=1}^{n_c}\alpha_{i,k-i}\Lambda_{k,i}\eta_i}_{\mathscr{L}_{\mathscr{A}}} + \underbrace{\sum_{i=k+1}^{n_c}\gamma_{i,k}B_i\eta_i}_{\mathscr{G}_{\mathscr{B}}} - \underbrace{B_k\eta_k}_{\mathscr{L}_{\mathscr{B}}}, \quad (1)$$

where $\mathscr{G}_{\mathscr{A}}$ and $\mathscr{L}_{\mathscr{A}}$ are the gain and loss in η_k due to aggregation, and $\mathscr{G}_{\mathscr{B}}$ and $\mathscr{L}_{\mathscr{B}}$ are the gain and loss in η_k due to breakup. Mass is explicitly conserved as $\sum_{k=1}^{n_c}\eta_k k M_p = \text{const}$ is prescribed, with M_p the primary particle mass.

Aggregation in $\mathscr{G}_{\mathscr{A}}$ and $\mathscr{L}_{\mathscr{A}}$ multiplicatively depend on a collision frequency $\Lambda_{i,j}$ expressing the rate at which two particles of sizes L_i and L_j collide, and a collision efficiency α expressing the likelihood for them to attach after collision. The collision frequency $\Lambda_{i,j}$ can be expressed as a linear superposition of the contributions due to Brownian motion, differential settling and turbulent shear (e.g., Hunt, 1980; Saffman and Turner, 1956; Serra and Casamitjana, 1998a).

However, Brownian motion can be neglected compared to turbulent shear in dynamical environments, e.g., estuaries and rivers (e.g., McCave, 1984), as well as differential settling because of strong hydrodynamic shielding between approaching particles (Stolzenbach and Elimelech, 1993). The simplified collision function $\Lambda_{i,j}$ is

$$\Lambda_{i,j} = \frac{G}{6}(L_i + L_j)^3. \tag{2}$$

The collision efficiency $\alpha_{i,j}$ in Eq. (1) is written as a function of the sizes of two colliding particles (Pruppacher and Klett, 1978; Friedlander, 1957), but the effect of floc porosity is introduced via the capacity dimension d_0. When organic matter and microbial biomass are absent or present at low concentrations, floc porosity tends to decrease the hydrodynamic shielding due to flow through the porous structure of the flocs (Kim and Stolzenbach, 2004; Kim and Yuan, 2005a; Kim and Yuan, 2005b; Sterling et al., 2005). For negligible concentrations of organic matter as in our laboratory experiment, the collision efficiency α can be therefore written as

$$\alpha_{i,j} = A\left(\frac{9}{d_{0,i}d_{0,j}}\right)\frac{(L_i/L_j)^2}{2(1+L_i/L_j)^2} \quad \text{with } L_i/L_j \leqslant 1, \tag{3}$$

where A is a calibration parameter. This expression for α is such that the sticking probability between any two flocs increases with floc sizes L_i and L_j increasing and with the ratio L_i/L_j decreasing.

Breakup in terms $\mathscr{G}_{\mathscr{B}}$ and $\mathscr{L}_{\mathscr{B}}$ is proportional to a breakup frequency B_i, expressing the rate at which flocs break up due to turbulence shear rate, which is modelled with the parametric expression by Winterwerp (1999)

$$B_i = E\left(\frac{\mu}{F_y}\right)^{1/2} G^{3/2} L_i \left(\frac{L_i}{L_p} - 1\right)^{3-d_{0,i}}, \tag{4}$$

where E is a calibration parameter, $F_y = O\{10^{-10}\}$ N is an estimate floc strength, L_p is the primary particle size, and the dimensionless term $(L_i/L_p - 1)^{3-d_0}$ states that increases in d_0 yield lower breakup frequency because flocs become more compact (e.g., Winterwerp, 2002). Breakup in $\mathscr{G}_{\mathscr{B}}$ is also proportional to a breakup distribution function $\gamma_{i,k}$ expressing how daughter flocs are distributed in size after breakup. At present, there are no clear experimental evidences of the effective shape of $\gamma_{i,k}$ for real flocs, and some hypotheses of binary, ternary and binomial breakup distributions have been proposed (e.g., Spicer and Pratsinis, 1996; Flesch et al., 1999; Serra and Casamitjana, 1998a). However, a binomial distribution, used to approximate a normal distribution, can be assumed to be generally valid for the central limit theorem as long as the number of independent breakup events is much larger than 1:

$$\gamma_{i,k} = \binom{i}{k} \Big/ \sum_{k=1}^{i} \binom{i}{k}. \tag{5}$$

Moreover, this distribution has recently been shown to generally give better results than binary and ternary distributions (Mietta et al., 2005). Therefore, Eq. (5) will be used in a Monte Carlo extraction to model stochastic breakup.

While the model structure allows to implement other contributions to aggregation and breakup, such as differential settling, biogenic aggregation, and non-linear breakup due to multiple collision, in the present work we focus on turbulence-induced collision and breakup processes for mathematical simplicity.

Flocs are considered as fractal bodies whose number of primary particles k and size L are related by the scaling law $k = (L/L_p)^{d_0}$, with d_0 the 3D capacity dimension used to characterise the floc structure (Vicsek, 1992). Several experimental observations have shown that, for instance, increases in d_0 can be caused by increases in breakup rate due to increases in shear rate (e.g., De Boer et al., 2000; Stone and Krishnappan, 2003; Chakraborti et al., 2003), or by processes of geometrical restructuring from mid to high shear rates (e.g., Thill et al., 2001; Spicer et al., 1998; Oles, 1992; Jullien and Meakin, 1989), whereas decreases in d_0 can be caused by a relaxation of particle–particle surface bonds due to a decrease in electrolyte concentration (e.g., Van Leussen, 1994; Berka and Rice, 2005). Yet, these changes in d_0 are assumed to apply to the entire collection of flocs is suspension.

Though d_0 = const has widely been used to describe self-similar structures resulting from aggregation of fine particles (e.g., Meakin, 1991), (statistical) self-similarity has experimentally been observed to hold over a floc size range of approximately one order only (e.g., Spicer et al., 1998; Johnson et al., 1996; Neimark et al., 1996). As kaolinite minerals and primary particles are crystalline and massive bodies with $d_0 = 3$, while suitably large flocs are porous and irregularly-structured bodies with $d_0 < 3$, floc geometry experiences a transition during growth from Euclidean to fractal. It appears therefore questionable whether the entire size evolution of cohesive sediment flocs can be modelled with an invariant scaling law (d_0 = const) from the size of the primary particle (microns) to the one of fully developed flocs (millimeters). Earlier experimental data show that the average 3D capacity dimension changes with time (Gardner et al., 1998), and that the average 2D capacity dimension gradually decreases as flocculation proceeds in time, i.e., for flocs growing in size (Chakraborti et al., 2003).

Experimental data collected in the settling column of Fig. 1 for flocs recorded at times $t = \{0, 3, 162, 165\}$ h, where $t = 0, 3$ h correspond to flocs in the non-equilibrium flocculation transition, while $t = 162, 165$ h correspond to flocs at steady state flocculation, have been processes as described in Maggi and Winterwerp (2004) to estimate the 3D capacity dimension d_0^*. These data, represented in Fig. 2, suggest the capacity dimension to decrease with increasing dimensionless size ℓ, meaning that flocs appear increasingly clustered or filamentous as L increases. The double-logarithmic scale suggests d_0 to follow a power-law of L:

$$d_0 = \delta \ell^{\xi} = \delta\left(\frac{L}{L_p}\right)^{\xi}, \tag{6}$$

where δ and ξ are estimated by data fitting (Table 1). The parameter δ can be interpreted as the capacity dimension of the primary particles, and it amounts to about $\delta = 3$, Table 1. The parameter ξ, instead, represents the rate at which d_0 decreases for $L > L_p$ and, as suggested by Table 1, can be taken $\xi = -0.1$. These values of δ and ξ are valid

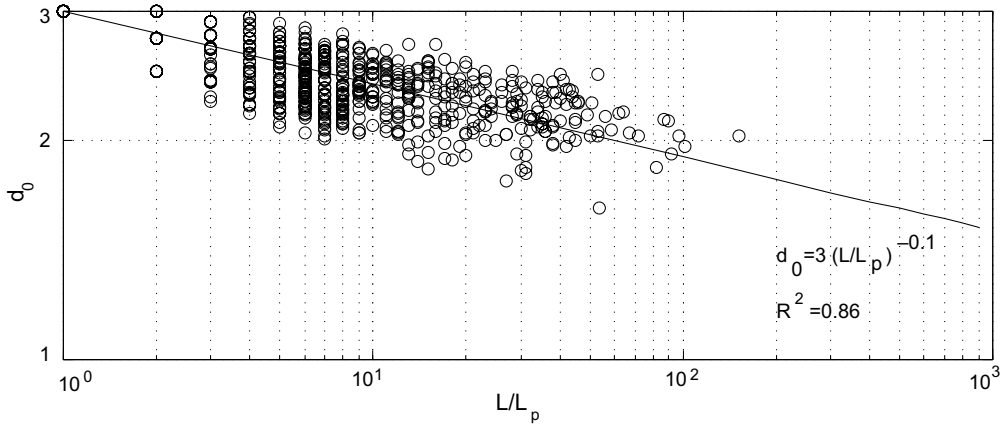

Figure 2 Relationship between the dimensionless size $\ell = L/L_p$ and the 3D capacity dimension d_0 of flocs observed in the settling column of Fig. 1.

Table 1 Values of δ and ξ resulting from least squares fitting to the data at times $t = \{0, 3, 162, 165\}$ h

Time t [h]	0	3	162	165
State	NE	NE	SS	SS
δ	3.437	3.378	3.357	3.359
ξ	−0.112	−0.079	−0.093	−0.092
R^2	0.847	0.830	0.863	0.859

NE and SS refer to non-equilibrium and steady state, respectively.

for flocculated kaolinite minerals, and correlate to experimental data with an $R^2 = 0.859$. Nevertheless, Eq. (6) allows to use other values of ξ to describe in a better way the decay in d_0 for suspensions of different nature, as well as a $\xi = 0$ and $\delta < 3$ when all flocs and primary particles are characterised by an identical capacity dimension $d_0 = \delta < 3$. Note that δ and ξ are substantially invariant in time, i.e., they do not change during the phase transition of the floc population from non-equilibrium to steady state. Furthermore, it is interesting to note that this finding is confirmed by recent analyses in Khelifa and Hill (2006), who derived a power-law similar to Eq. (6) not from direct analysis of floc geometry but from settling velocity data.

The scaling law relating the size and primary-particle number of growing flocs is therefore expressed as

$$k = (L/L_p)^{\delta(L/L_p)^{\xi}}, \tag{7}$$

which allows to determine the size L of a floc given k, L_p, ξ and δ. The floc sizes L_k so computed are then used to determine $\Lambda_{k,j}$, $\alpha_{k,j}$ and B_k of Eqs. (2)–(4).

Eq. (6) is limited to the range of $\ell = L/L_p$ for which $1 \leqslant d_0 \leqslant 3$, where the upper boundary is obvious for physical reasons, and the lower boundary is due to the fact that flocs with $d_0 < 1$ would be two disjoint masses rather than a unique floc. In the upper boundary, onset of flocculation is characterised by flocs that experience a crossover from Euclidean to fractal structure occurring as soon as ℓ becomes $\ell > 1$. The Euclidean-to-fractal crossover may be characterised by a discontinuity not included in Eq. (6). Consider n primary particles to attach forming a linelike chain with dimensionless linear size $\ell = L/L_p = n$; the capacity dimension of this newly formed floc will be $d_0 = \log[n]/\log[n] = 1$, that is smaller than $d_0 = 3n^{-0.1}$ for n small. However, the probability that all primary particles collide to form one such string is very low for particulate systems in turbulent fields. In addition, this is expected to occur only for n close to 2 and to vanish quickly during the initial exponential growth phase without interfering with the time and length scales of flocculation reactions. Similarly, if we consider monosized primary particles with $L_p = 5$ μm, the size L^* corresponding to the lower boundary ($d_0 = 1$) is $L^* = L_p(1/\delta)^{1/\xi} = 5 \cdot 5.9 \times 10^{-2}$ m ≈ 30 cm. This size is not reached by real sediment flocs in natural conditions therefore Eq. (6) can describe decreases in d_0 over a broad range of floc sizes in real conditions.

A more interesting aspect is that Eq. (6) describes the Euclidean-to-fractal transition of floc structure (Maggi, 2007) and the increase in floc porosity without the single or multiple discontinuities introduced in ''core-shell'' models (e.g., Kunster et al., 1997; Wu et al., 2002; Veerapaneni and Wiesner, 1996; Li and Logan, 2001). In addition, if the floc size is assumed to scale as $L \propto G^x$ with $x < 0$ (e.g., Lick et al., 1993), then from Eq. (6) we can write $d_0 \propto G^{x\xi}$ where the product $x\xi > 0$ signifies that increases in G correspond to increases in d_0; this type of scaling has been observed by Chakraborti et al. (2003) in representing the 2D floc capacity dimension for a variety of some shear rate values.

While the physical process responsible for the formation of fractal structure from Euclidean particles can be related to shielding effects (e.g., Ball and Blunt, 1989), that is internal throats of flocs are less accessible to particles than the surface, the decrease in capacity dimension with increasing floc size can be related to a gradual transition from Brownian flocculation at initial states (i.e., when small

particles collide and attach prevalently due to Brownian diffusivity), toward cluster–cluster flocculation (i.e., when larger flocs collide and attach mainly due to shear flow and differential settling, Farley and Morel, 1986; Burd and Jackson, 1997). These two regimes can be associated to DLA and CCA processes respectively, which result in the formation of randomly-structured fractal flocs well-known to be characterised by 3D capacity dimensions d_0 (DLA) ≈ 2.5 and d_0(CCA) ≈ 1.8 (e.g., Weitz et al., 1985; Vicsek, 1992; Meakin, 1983).

Although the effective nature and features of the Euclidean-to-fractal crossover are still source of ample debate from pattern formation to non-linear dynamics, which are beyond the scope of this paper, Eq. (6) can be considered a simplified nonetheless physically representative formulation to describe the observed changes in fractal attributes of sediment flocs during growth. This further allows us to put forth and test hypotheses on the feedback between the fractal dimension of flocs and the aggregation and breakup kinetics, and its impact on the floc size distribution in simplified mathematical terms.

Model calibration and validation

The solution of the PBE in Eq. (1), computed numerically via an implicit finite-difference technique, is integrated over a number of classes n_c arbitrarily taken large enough not to limit the maximum floc size (unknown *a priori*), and with a time step $\Delta t \propto 1/G^{3/2}$ kept constant during integration. The floc primary-particle number concentrations η_k, associated to the floc sizes L_k, are grouped into $N_c < n_c$ size-based classes arranged in a geometrical series of L, which are next normalised to obtain the computed FSDs $p^*(L)$.

The calibration of the model has been performed by determining the parameters A and E in Eqs. (3) and (4) which minimise the error function defined as the distance between the computed $p^*(L)$ and experimental $p(L)$:

$$e = \frac{1}{2}\sum_{i=1}^{N_c} |p_i^*(L) - p_i(L)|, \tag{8}$$

with $0 \leqslant e \leqslant 1$. To this end, the two-dimensional Downhill Simplex Method (Press et al., 1992) is used to minimise e against the experimental FSDs corresponding to $G = \{10, 40\}\,\mathrm{s}^{-1}$, Fig. 3(a). Calibration resulted in $A = 1.68$ and $E = 1.4 \times 10^{-4}$. A comparison between computed and experimental FSDs in Fig. 3(b), used for validation, shows that the overall shape of the FSDs is qualitatively well predicted in both cases of $G = 5\,\mathrm{s}^{-1}$ and $G = 20\,\mathrm{s}^{-1}$. The better prediction for $G = 20\,\mathrm{s}^{-1}$ is expected because it is a case of interpolation between calibration values of G, while $G = 5\,\mathrm{s}^{-1}$ is a case of extrapolation. Though not perfect, the model seems appropriate to study the effect of various physical parameters.

Modelling the floc size distribution for various mass concentrations and shear rates

Flocculation of cohesive sediment in natural conditions has widely been documented to produce larger flocs for increas-

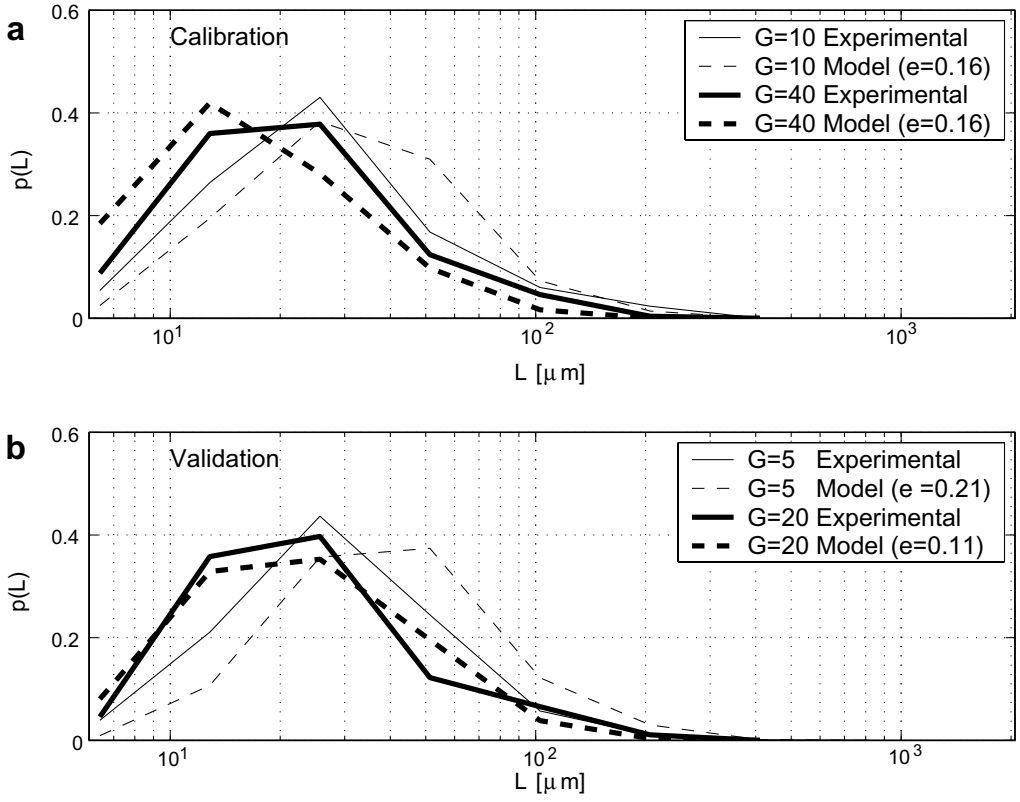

Figure 3 Comparison between steady state experimental and simulated FSDs from (a) calibration and (b) validation of the model for sediment concentration $c = 0.5$ g/l and various values of shear rate G.

ing mass concentrations, as well as for decreasing turbulent shear rate. This behavior is intimately related to the rate of aggregation and breakup processes, and their balance.

As aggregation and breakup in Eq. (1) are related to the total number concentration η_T via $\mathscr{G}_{\mathscr{A}}$ and $\mathscr{L}_{\mathscr{A}}$, which scale as $\eta_T^2 \propto c^2$, and via $\mathscr{G}_{\mathscr{B}}$ and $\mathscr{L}_{\mathscr{B}}$, which scale as $\eta_T \propto c$, larger flocs are expected when c increases. Fig. 4(a) resumes results from five runs with $c = \{0.2, 0.5, 1, 1.5, 2\}$ g/l and $G = 10\ s^{-1}$ showing that the model reproduces mentioned behavior properly, and confirms our expectations and early laboratory and field observations (e.g., Rahmani et al., 2003; Serra and Casamitjana, 1998b).

Aggregation and breakup are also related to the shear rate G since $\mathscr{G}_{\mathscr{A}}$ and $\mathscr{L}_{\mathscr{A}}$ scale as G, while $\mathscr{G}_{\mathscr{B}}$ and $\mathscr{L}_{\mathscr{B}}$ scale as $G^{3/2}$. From a physical point of view, low values of G, implying low particle circulation and collision, and low shear stresses and breakup frequency, would presumably lead to right-skewed FSDs. In contrast, increases in G, implying higher shear stresses, would likely lead to high breakup frequency and left-skewed FSDs. Fig. 4(b), which represents results for $G = \{5, 10, 20, 40, 80, 160\}\ s^{-1}$, shows that our model predicts this behavior in a wide range of shear rates, and agrees qualitatively with theoretical and experimental data (e.g., Rahmani et al. (2003), Spicer and Pratsinis (1996), Oles (1992), Dyer (1989)).

These results show that the overall dynamical pattern of the model in Eq. (1) is consistent with prior experiences, making it reliable for further analyses on the feedback between aggregation and breakup processes and floc structure.

Analyses of flocculation reactions and floc geometry

The interplay between the processes of aggregation and breakup and the geometrical properties of the flocs, and its impact on the floc size distribution are analysed by comparing our experimental and model results for two hypotheses of flocculation reactions, i.e., semi-stochastic and deterministic, and two hypotheses of floc capacity dimension, i.e., constant and variable.

Semi-stochastic and asymmetric reactions with variable floc capacity dimension

The most general case described by Eq. (1) comprises the use of deterministic aggregation and stochastic breakup, and variable capacity dimension described by Eq. (6). These kinetics yield asymmetric flocculation reactions because aggregation occurs among flocs belonging to any class, and breakup returns daughter flocs randomly (binomially) distributed in mass, with no memory of the aggregation processes that formed them. These types of reactions (i.e., semi-stochastic and asymmetric), and this description of the evolution of floc geometry (i.e., variable capacity dimension) are expected to affect flocculation and the full floc size distribution. In fact, an increasing floc mass during growth corresponds to a floc size increasing more rapidly for a decreasing capacity dimension than for a constant dimension, resulting in a collision frequency and efficiency that

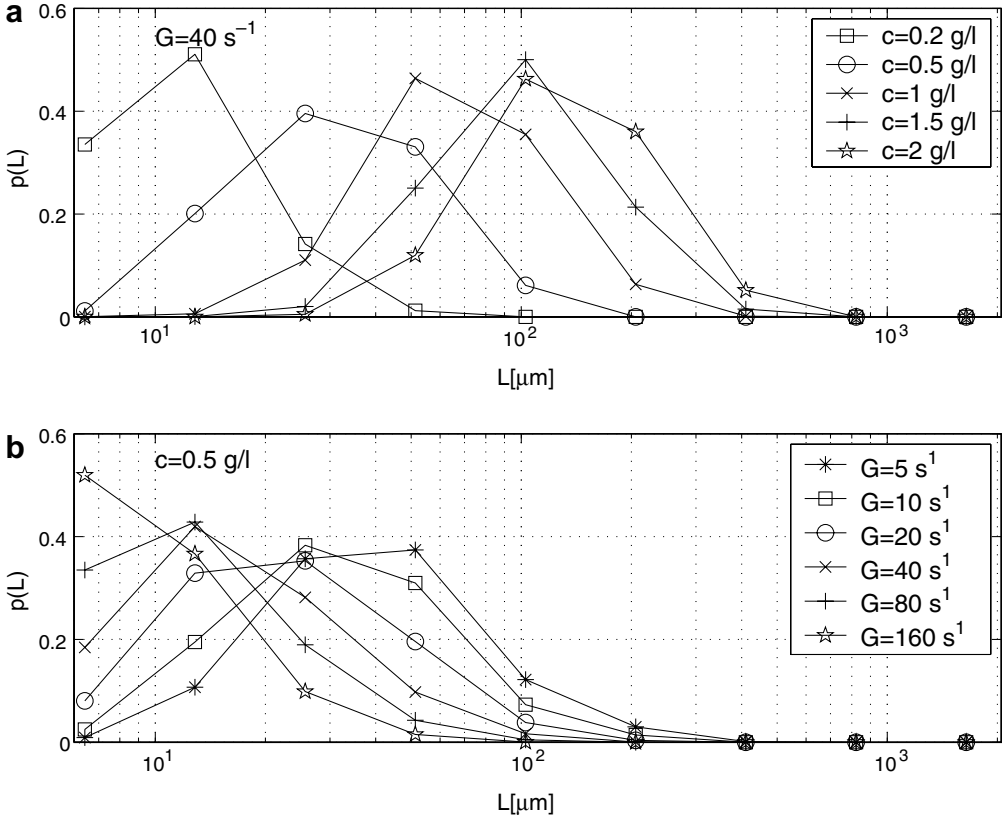

Figure 4 Steady state FSDs computed with Eq. (1) (a) for various values of sediment mass concentration c and (b) for various values of shear rate G.

increase more rapidly. Furthermore, a capacity dimension decreasing with an increasing floc mass implies a floc strength that decreases more rapidly than for a constant capacity dimension, thus yielding an increasing breakup rate in Eq. (4).

The rate at which the scaling relationship between floc mass and size changes during growth, and the rate at which the reactions of aggregation and breakup change with floc sizes, depends on the exponent ξ and the factor δ of Eq. (6).

The simulations for various values of ξ and δ = const = 3, shown in Fig. 5(a), highlight that the equilibrium FSD becomes slightly more right-skewed for ξ decreasing from $\xi = -0.05$ to $\xi = -0.11$, i.e., with steeper slopes $\mathrm{d}d_0/\mathrm{d}\ell$. This is due to the fact that the number of primary particles needed to build a floc of size L decreases for d_0 decreasing. As the total number of primary particles in the control volume is constant, a decrease in d_0 is accompanied by an increase in particle number concentration. Since aggregation in Eq. (1) scales with power two of the particle number concentration (see Section ''Modelling the floc size distribution for various mass concentrations and shear rates''), aggregation becomes more important than breakup, which scales linearly with the number concentration, and the resulting FSD becomes right-skewed.

This phenomenon is more evident for increasing values of shear rate, Fig. 5(b). In particular, at high values of ξ (i.e., close to zero), the floc size distribution appears more left-skewed at $G = 40\ \mathrm{s}^{-1}$ than at $G = 10\ \mathrm{s}^{-1}$, and more right-skewed at $G = 40\ \mathrm{s}^{-1}$ compared to the ones at $G = 10\ \mathrm{s}^{-1}$ for very small values of ξ. This means that any variation in rate of change of capacity dimension can exert a strong influence on the steady state floc size distribution, and that this influence is more pronounced for increasing turbulence shear rates. It is worth noting that the lowest errors e are found for ξ between -0.1 and -0.08 for both G-values, whereas either smaller or higher values of ξ result in larger deviations from experimental observations. This may indicate that the exponent ξ is independent from G.

Homogeneous sediment has been used so far in our model and experiments: however, sedimentological properties of real suspensions can vary across the water column in mineral composition and organic content. Although the effect of sediment and organic matter heterogeneity is beyond the scope of this paper, it is worth highlighting some key aspects. Depending on background processes and the local hydrodynamic characteristics of a site, the organic and nutrient contents can vary largely, i.e., high near the water surface (due to the presence of algal flora) and near the bed (due to benthic microorganisms). Analogously, mineral composition can be characterised by stratification across the water column, with fine particles in suspension and coarser particles close to the bed. These heterogeneities can be case of spatial variability in ξ; as this is difficult to detect, a specific experiment should be designed to study these effects.

The mass-size scaling law and the flocculation reactions depend also on the fractal dimension δ of the primary particles in Eq. (6). Our simulations for variable δ and ξ = con-

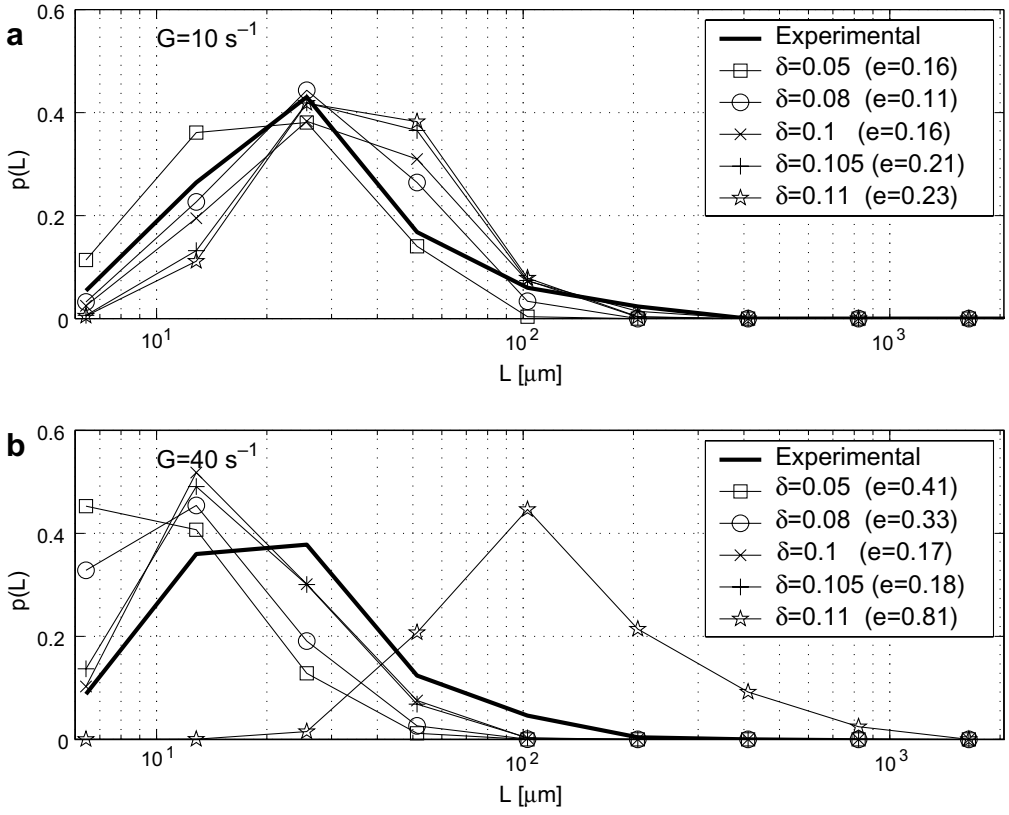

Figure 5 Steady state FSDs computed for various ξ and $\delta = 3$, and for two values of shear rate G in the case of semi-stochastic and asymmetric reactions.

st = −0.1 show that, at low shear rates, a decrease in δ has an effect on the equilibrium FSD similar to the one of decreasing ξ, i.e., producing more right-skewed FSDs, Fig. 6(a). However, this is more pronounced than in the case of variations in ξ; an explanation has been found in that d_0 computed for decreasing δ is generally lower than the one computed with variable ξ (data not shown). These lower values of capacity dimension call back the mechanism introduced before to explain the gradual shaping into right-skewed FSDs. Higher shear rates G, Fig. 6(b), do not produce further variations of skewness compared to the ones of Fig. 6(a). In other words, relatively small variations in primary particle capacity dimension δ appear to be quite important for the floc size distribution, generally causing more right-skewed distributions as δ decreases, and regardless of the environmental forcing, meaning that δ does describe a sediment property mainly.

We note that the error e for $\delta = 2.9$ is the lowest found in our simulations. This may suggest that the effective capacity dimension of kaolinite primary particles is slightly lower than the one used in the model ($\delta = 3$).

These results indicate that the shape of the steady state floc size distribution can strongly be affected by the properties of the mineral. In fact, while kaolinite used in our experiments and model is characterised by regular and massive crystals with δ close to 3, other minerals suspended in natural waters, such as illite and montmorillonite for example, have different crystal geometry (porous), with much lower capacity dimension δ. This suggests that the model for variable fractal dimension proposed here can be more flexible than a model that uses a constant (average) capacity dimension for all flocs and primary particles because it can take into account variability in fractal properties from the mineral to the floc sizes.

Semi-stochastic and asymmetric reactions with invariant floc capacity dimension

A simplified version of Eq. (1) is examined; here, semi-stochastic and asymmetric aggregation and breakup reactions are as in Section ''Semi-stochastic and asymmetric reactions with variable floc capacity dimension'', but the floc capacity dimension is hypothesised to be constant like, for instance, in Flesch et al. (1999) and Zhang and Li (2003). This hypothesis is equivalent to use Eq. (6) with $\xi = 0$ and $d_0 \equiv \delta = \text{const}$.

The effect of using a capacity dimension constant with the floc size is shown in Fig. 7 for various values of $d_0 \equiv \delta$ and various values of G. Also in this case, as in the previous numerical analyses, a decrease in d_0 corresponds to an equilibrium FSD more right-skewed. Panels (a) and (b) in Fig. 7 show that this effect is substantially invariant with the shear rate G. In addition, it appears from both panels that decreases in d_0 below a threshold value, approximately between 1.7 and 1.8, causes the floc size distribution to abruptly become highly right-skewed. This may be explained by the fact that $d_0 = \text{const}$ describes the fractal dimension of all flocs at any size, whereas the model in

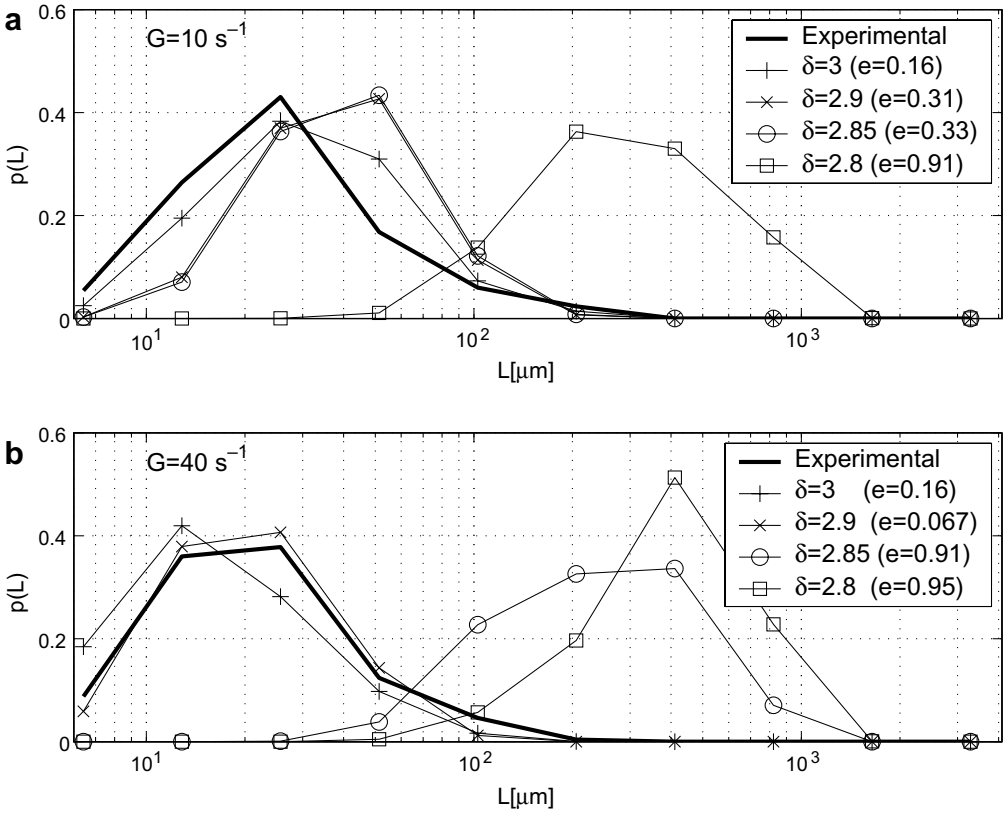

Figure 6 Steady state FSDs computed for various primary particle capacity dimension δ and $\xi = -0.1$, and for two values of shear rate G in the case of semi-stochastic and asymmetric reactions.

Eq. (6) takes into account a gradual decrease in d_0 for increasing floc size, presumably smoothing out rapid transitions in the overall flocculation dynamics.

Values of d_0 in the range 2–2.3, generally used when modelling cohesive sediment flocs with constant capacity dimension, have produced FSDs very similar to experimental ones at $G = 40\ s^{-1}$, with a minimum error of $e = 0.09$, Fig. 7(b). However, this error e increases up to $e = 0.5$ for $d_0 = 2$ and $G = 10\ s^{-1}$ in Fig. 7(a). It is worth noting that, in contrast, errors obtained from Eq. (6) with $\xi = -0.1$ and $\delta = 3$ at both $G = 10\ s^{-1}$ and $G = 40\ s^{-1}$ are all close to $e = 0.16$ or less, such as in the case of Fig. 6(b). This and the previous analyses show therefore that a fractal dimension changing with the floc size produces less erroneous predictions of the floc size distribution, and that this passes through the use of the parameters δ and ξ.

Deterministic and symmetric reactions with invariant floc capacity dimension

In this section we analyze the interplay between aggregation and breakup processes and the geometrical properties of the flocs in the case of deterministic and symmetric reactions following from Krone's hypotheses of ''particle aggregation order'', and constant capacity dimension for all flocs (Krone, 1963). This type of reactions imply that aggregation occurs among flocs from the same class, and breakup releases the forming flocs (memory effect), and that the floc size changes in a fully multiplicative fashion (via a constant scaling) during aggregation and breakup because of $d_0 = \text{const}$. To this end, some important simplifications in the model of Eq. (1) are adopted. The floc mass M after w aggregation steps is $p^w M$, where $p = \text{const}$ represents the number of lower-order flocs integrating into the newly formed floc. Similarly, w breakup events of a floc of mass M returns p^w flocs of mass $1/p^w M$. Assuming $p = 2$ (i.e., binary breakup), this model can be written as

$$\frac{d\eta_i}{dt} = \frac{1}{2}\alpha\Lambda_{i-1,i-1}\eta_{i-1}^2 - \alpha\Lambda_{i,i}\eta_i^2 + 2B_{i+1}\eta_{i+1} - B_i\eta_i, \tag{9}$$

where the index $_i$ refers to the number concentration η_i of aggregates made of 2^{i-1} primary particles, $\gamma_{i,i-1}^{(\mathrm{Bin})} = 2$ in $\mathscr{G}_{\mathscr{B}}$ is the binary breakup, and with all other terms as in Eq. (1) and $d_0 = 2$. Calibration of the population balance in Eq. (9) gives the optimal values $A = 1$ and $E = 1.44 \times 10^{-5}$, which are next used to compute to steady state FSD for various mass concentrations c and shear rates G.

The results in Fig. 8 show a monotonically decreasing floc size distribution in all tested conditions of sediment concentration (panel a) and shear rate (panel b), whereas all our experimental FSDs are non-monotonic.

From the different models of kinetics of aggregation and breakup processes and floc geometry used in this section and in Sections ''Semi-stochastic and asymmetric reactions with variable floc capacity dimension'' and ''Semi-stochastic and asymmetric reactions with invariant floc capacity dimension'', important aspects in modelling flocculation of cohesive sediment have been isolated and analysed.

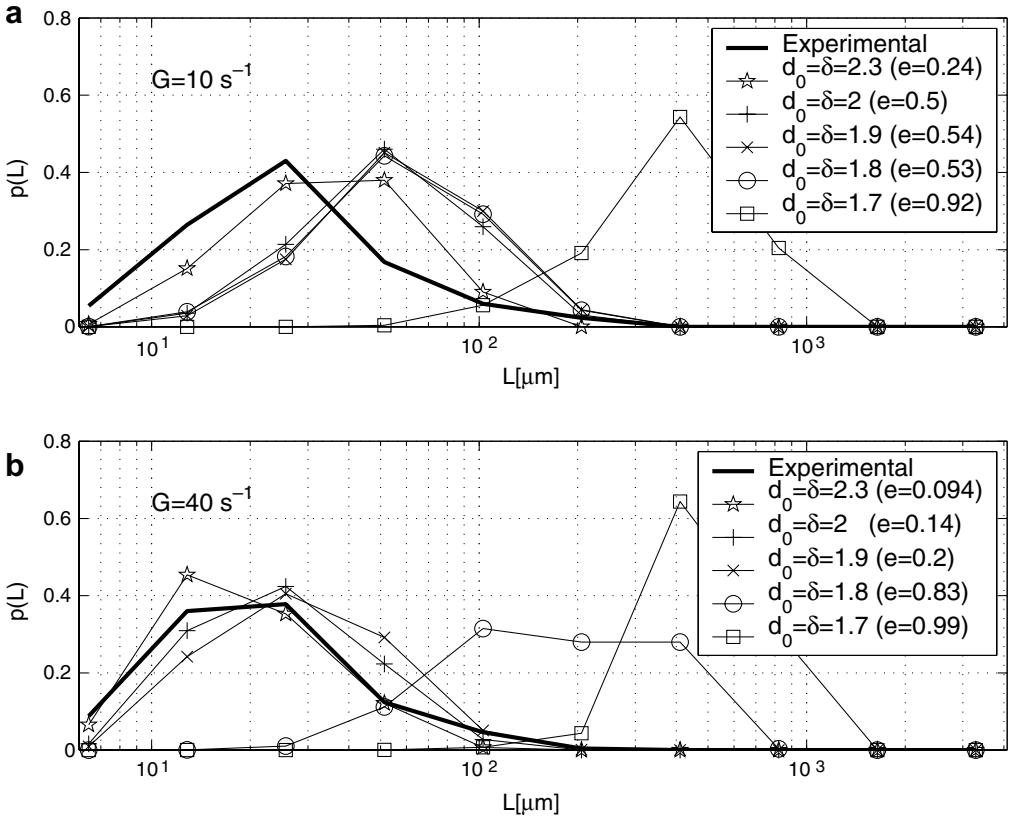

Figure 7 Steady state FSDs computed for various values of capacity dimension $d_0 = \delta = \text{const}$ in the case of semi-stochastic and asymmetric reactions, and for two values of shear rate G.

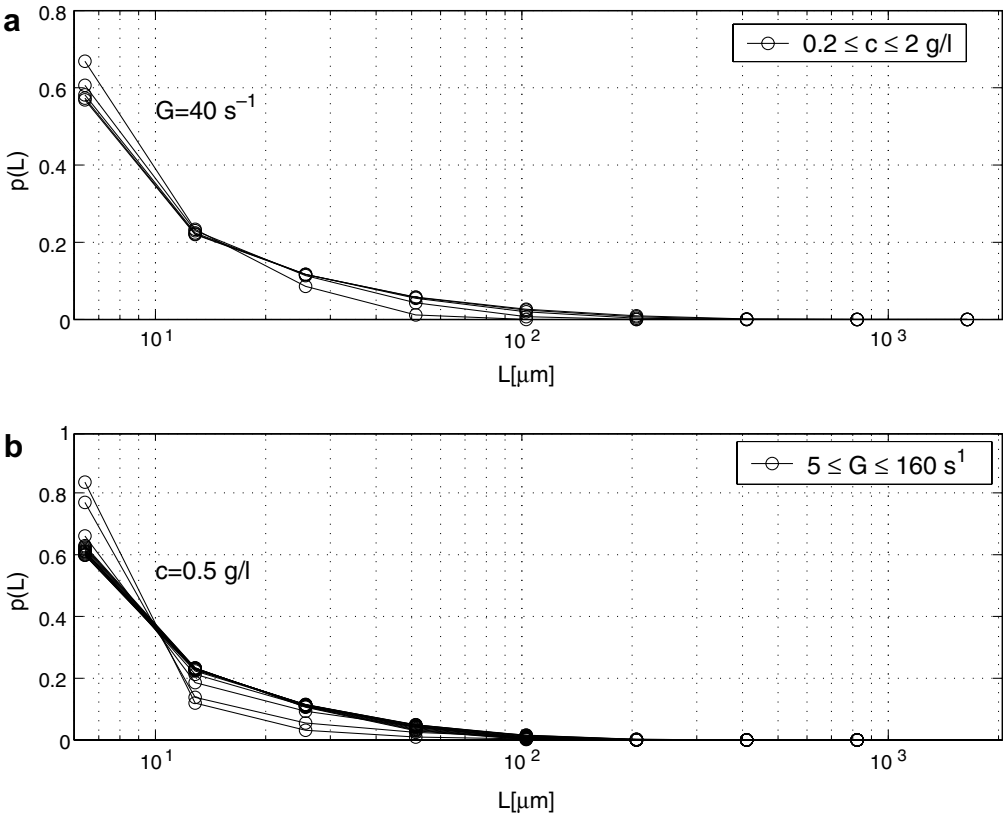

Figure 8 Steady state FSDs computed with the simplified model of Eq. (9) for (a) mass concentrations $c = \{0.2, 0.5, 1, 1.5, 2\}$ g l^{-1}, and (b) shear rates $G = \{5, 10, 20, 40, 80, 160\}$ s^{-1}.

While a variable capacity dimension has been shown to impact the statistical moments of a unimodal floc size distribution computed with semi-stochastic and asymmetric reactions, the use of symmetric and deterministic aggregation and breakup reactions causes the floc size distribution to be unconditionally monotonically decreasing regardless of the geometrical description of the flocs. The simplified kinematic model in Eq. (9) introduces large deviations from the experimental data that can be explained as the results of the kinetics of the reactions rather than the description of floc geometry.

Conclusions

This paper proposes a population balance equation to model flocculation of cohesive sediment flocs that are characterised by variable capacity dimension. The formulation to account for variations in capacity dimension is based on experimentally-acquired data and introduces a non-linearity in the aggregation and breakup reactions which, in turn, affects the equilibrium floc size distribution.

Our analyses quantitatively show that the steady state floc size distribution can be better modelled with semi-stochastic and asymmetric (rather than deterministic and symmetric) aggregation and breakup reactions, and with variable (rather than constant) floc capacity dimension. In particular, the power-law used to take into account the variations in capacity dimension during flocculation results in lower errors. This can be attributed to a higher accuracy in describing the fractal attributes of flocs over the two orders of magnitude in floc size observed experimentally, and to a higher accuracy in describing the fractal properties of the primary particles. This makes this population balance equation a more precise tool to study numerically the floc size distributions observed experimentally at different shear rates compared to models that use a constant capacity dimension.

Despite promising results, more comprehensive experimental data sets are needed for a better calibration of the model and a more extensive analysis of it, especially for more values of shear rates, mass concentrations and sediment type. For this reason, we aim at collecting more data from both laboratory and field campaigns, and use our new model for calibration and predictions of flocculation of cohesive sediment in real the real world as well as settling column tests.

Acknowledgment

This work has been supported by the Delft University of Technology Research Funds through the BEO-Program.

References

Ball, R., Blunt, M., 1989. Screening in multifractal growth. Physical Review A 39 (7), 3591—3596.

Berka, M., Rice, J.A., 2005. Relation between aggregation kinetics and the structure of kaolinite aggregates. Langmuir 21, 1223–1229.

Burban, P.Y., Lick, W., Lick, J., 1989. The flocculation of fine-grained sediments in estuarine waters. Journal of Geophysical Research – Oceans 94 (4), 514–523.

Burd, A., Jackson, G.A., 1997. Predicting particle coagulation and sedimentation rates for a pulsed input. Journal of Geophysical Research – Oceans 102 (C5), 10545–10561.

Chakraborti, R.K., Gardner, K.H., Atkinson, J.F., van Benschoten, J.E., 2003. Changes in fractal dimension during aggregation. Water Research 37, 873–883.

De Boer, D.H., Stone, M., Lévesque, L.M.J., 2000. Fractal dimensions of individual flocs and floc population in streams. Hydrological Processes 14, 653–667.

Dyer, K.R., 1989. Sediment processes in estuaries: future research requirements. Journal of Geophysical Research 94(c10) (14), 327–332.

Farley, K.J., Morel, F.M.M., 1986. Role of coagulation in the kinetics of sedimentation. Environmental Science and Technology 20, 187–195.

Flesch, J.C., Spicer, P.T., Pratsinis, S.E., 1999. Laminar and turbulent shear-induced flocculation of fractal aggregates. American Institute of Chemical Engineers 45 (5), 1114–1124.

Friedlander, S.K., 1957. Mass and heat transfer to single spheres and cylinders at low Reynolds number. American Institute of Chemical Engineers 3, 43–48.

Friedlander, S.K., 1977. Smoke, Dust and Haze, fundamentals of aerosol behavior. Wiley, New York.

Gardner, K.H., Theis, T.L., Young, T.C., 1998. Colloid aggregation: numerical solution and measurements. Colloids and Surfaces A 141, 237–252.

Hunt, J.R., 1980. Prediction of oceanic particle size distribution from coagulation and sedimentation mechanisms. In: Kavanaugh, M.D., Kekie, J.T. (Eds.), Advances in Chemistry 189 – Particle in Water. American Chemical Society, pp. 243–257.

Johnson, C.P., Li, X., Logan, B.E., 1996. Settling velocities of fractal aggregates. Environmental Science and Technology 30, 1911–1918.

Jullien, R., Meakin, P., 1989. Simple models for the restructuring of three-dimensional ballistic aggregation. JCIS 127, 265–272.

Khelifa, A., Hill, P.S., 2006. Models for effective density and settling velocity of flocs. Journal of Hydraulic Research 44, 390–401.

Kim, A.S., Stolzenbach, K.D., 2004. Aggregate formation and collision efficiency in differential settling. Journal of Colloid and Interface Science 271, 110–119.

Kim, A.S., Yuan, R., 2005a. Hyrodynamics of an ideal aggregate with quadratically increasing permeability. Journal of Colloid and Interface Science 285, 627–633.

Kim, A.S., Yuan, R., 2005b. Anew model for calculating specific resistance of aggregated colloidal cake layers in membrane filtration processes. Journal of Membrane Science 249, 89–101.

Krishnappan, B.C., 1990. Modelling of settling and flocculation of fine sediments in still water. Canadian Journal of Civil Engineering 17, 763–770.

Krone, R.B., 1963. A study of rheologic properties of estuarial sediments Tech. Bul. 7. USAE Comm. on Tidal Hydr., Vicksburg, MS.

Kunster, K.A., Wijers, J.G., Thoenes, D., 1997. Aggregation kinetics of small particles in agitated vessels. Chemical Engineering Science 52 (1), 107–121.

Lee, S.I., Seo, I.S., Koopman, B., 1997. Effect of mean velocity gradient and mixing time on particle removal in seawater induced flocculation. Water, Air and Soil Pollution 78, 179–188.

Li, X.-Y., Logan, B.E., 2001. Permeability of fractal aggregates. Water Research 35 (14), 3373–3380.

Lick, W., Huang, H., Jepsen, R., 1993. Flocculation of fine-grained sediments due to differential settling. Journal of Geophysical Research 98(C6) (10), 279–288.

Maggi, F., 2007. Variable fractal dimension: a major control for floc structure and flocculation kinematics of suspended cohesive sediment. J. Geophys. Res.. doi:10.1029/2006JC003951.

Maggi, F., Winterwerp, J.C., 2004. Method for computing the three-dimensional capacity dimension from two-dimensional projections of fractal aggregates. Physical Review E 69, 011405.

Maggi, F., Winterwerp, J.C., Fontijn, H.L., van Kesteren, W.G.M., Cornelisse, J.M., 2002. A settling column for turbulence-induced flocculation of cohesive sediments. In: Wahl, T.L., Pugh, C.A., Oberg, K.A., Vermeyen, T.B., (Eds.), Proceedings of HMEM2002 Conference, Estes Park, Colorado, paper 93. doi:10.1061/40655(2002)34.

Maggi, F., Manning, A.J., Winterwerp, J.C., 2006. Image separation and geometric characterisation of mud flocs. Journal of Hydrology 326, 325–348.

McCave, I.N., 1984. Size spectra and aggregation of suspended particles in the deep ocean. Deep-Sea Research 31 (4), 329–352.

Meakin, P., 1983. Diffusion-controlled cluster formation in two, three, and four dimensions. Physical Review A 27 (1).

Meakin, P., 1991. Fractals aggregates in geophysics. Reviews of Geophysics 29.

Mietta, F., Maggi, F., Winterwerp, J.C., 2005. Sensitivity to breakup functions in a population balance equation for cohesive sediments. In: Proceeding of the 8th INTERCOH Conference, Saga, Japan.

Neimark, A.V., Köylü, Ü.O., Rosner, D.E., 1996. Extended characterization of combustion-generated aggregates: self-affinity and lacunarities. Journal of colloid and Interface Science 180, 590–597.

Oles, V., 1992. Shear-induced aggregation and breakup of polystyrene latex particles. Journal of Colloid Interface Science 154, 351–358.

O'Melia, C., 1980. Aquasols: the behaviour of small particles in aquatic systems. ES&T 14 (9), 1052–1060.

Press, W.H., Flammery, B.P., Teukolsky, S.A., Vatterling, W.T., 1992. Numerical Recipes in Fortran: The Art of Scientific Computing, Second ed. Cambridge University Press, Cambridge, NY, USA.

Pruppacher, H.R., Klett, J.D., 1978. The Microphysics of Clouds and Precipitation. Reidel, Dordrecht.

Rahmani, N., Masliyah, J., Dabros, T., 2003. Characterization of asphaltenes aggregation and fragmentation in a shear field. AIChE Journal 49, 1645–1650.

Saffman, P.G., Turner, J.S., 1956. On the collision of drops in turbulent clouds. Journal of Fluid Mechanics 1, 16–30.

Sato, D., Kobayashi, M., Adachi, Y., 2004. Effect of floc structure on the rate of shear coagulation. JCIS 272, 345–351.

Serra, T., Casamitjana, X., 1998a. Structure of the aggregates during the process of aggregation and break-up under a shear flow. Journal of Colloid and Interface Science 206, 505–511.

Serra, T., Casamitjana, X., 1998b. Modelling the aggregation and break-up of fractal aggregates in shear flow. Applied Scientific Research 59, 255–268.

Spicer, P.T., Pratsinis, S.E., 1996. Universal steady state particle-size distribution. AIChE Journal 42 (6), 1612–1618.

Spicer, P.T., Pratsinis, S.E., Raper, J., Amal, R., Bushell, G., Meesters, G., 1998. Effect of shear schedule on particle size, density, and structure during flocculation in stirred tanks. Powder Technology 97, 26–34.

Sterling, M.C., Bonner, J.S., Ernest, A.N.S., Page, C.A., Autenrieth, R.L., 2005. Application of fractal flocculation and vertical transport model to aquatic sol-sediment systems. Water Research 39, 1818–1830.

Stolzenbach, K.D., Elimelech, M., 1993. The effect of particle density on collision between sinking particles: implications for

particle aggregation in the ocean. Deep-Sea Research I 41 (3), 469—483.

Stone, M., Krishnappan, B.G., 2003. Floc morphology and size distributions of cohesive sediment in steady flow. Water Research 37, 2739—2747.

Thill, A., Moustier, S., Aziz, J., Wiesner, M.R., Bottero, J.Y., 2001. Floc restructuring during aggregation: experimental evidence and numerical simulation. Journal of Colloid and Interface Science 243, 171—182.

Van Leussen, W., 1994. Estuarine Macroflocs. Ph.D. Thesis, University of Utrecht.

Veerapaneni, S., Wiesner, M.R., 1996. Hydrodynamics of fractal aggregates with radially varying permeability. Journal of Colloid and Interface Science 177, 45—57.

Vicsek, T., 1992. Fractal Growth Phenomena. World Scientific, Singapore.

von Smoluchowski, M., 1917. Versuch einer Mathematischen Theorie der Koagulations-kinetik Kolloid Losungen. Zeitschrift fur Physikalische Chemie 92, 129—168.

Weitz, D.A., Huang, J.S., Lin, M.Y., Sung, J., 1985. Limits of the fractal dimension for irreversible kinetic aggregation of gold colloids. Physical Review Letters 54 (13), 1416—1419.

Winterwerp, J.C., 1998. A simple model for turbulence induced flocculation of cohesive sediment. Journal of Hydraulic Engineering Research 36 (3), 309—326.

Winterwerp, J.C., 1999. On the dynamics of high-concentrated mud suspensions. Ph.D. Thesis, Delft University of Technology.

Winterwerp, J.C., 2002. On the flocculation and settling velocity of estuarine mud. Continental Shelf Research 22, 1339—1360.

Wu, R.M., Lee, D.L., Waite, T.D., Guan, J., 2002. Multilevel structure of sludge flocs. Journal of Colloid and Interface Science 252, 383—392.

Zhang, J.-J., Li, X.-Y., 2003. Modeling particle-size distribution dynamics in a flocculation system. American Institute of Chemical Engineers 49 (7), 1870—1882.